EFFECT OF FLIPPING ON FREE CONVECTIVE HEAT TRANSFER DURING MELTING OF A PHASE CHANGE MATERIAL IN CONCENTRIC HORIZONTAL ANNULI OF DIFFERENT CROSS-SECTION

by

D. B. Khillarkar, S. Devahastin and A. S. Mujumdar

Original scientific paper
UDC: 536.42:519.876.5
BIBLID: 0354–9836, 2 (1998), 2, 27–43

Results are presented of a finite element computational study of the free convection-dominated melting of a pure phase change material contained in concentric horizontal annuli of the following configuration:
(a) Square external tube with a circular tube inside – Annulus Type A
(b) Circular external tube with a square tube inside – Annulus Type B
Effect of heating the inside wall at a temperature above the melting point of the material was studied. Flow and temperature patterns within the melt, local heat flux distributions at the heating surface and the cumulative energy charged as a function of time are presented and discussed. The effect of flipping which involves inverting the container upside-down at pre-selected times after initiation of melting as a measure to increase the heat transfer rate during the later stage of the melting process is examined and discussed. It is shown that this simple yet effective technique presents a simple way to enhance the overall melting rate, i.e., the cumulative heat storage.

Introduction

Convection-dominated melting of a phase change material (PCM) has been studied for various geometric configurations. However, particular attention is given to melting in a horizontal annulus as a model for a latent heat thermal energy storage system. A number of numerical/analytical studies [1–3] have been performed in an attempt to model the melting phenomenon based on the Boussinesq approximation. Rieger *et al.* [4] and Ho and Viskanta [5] investigated experimentally the evolution of the solid-liquid interface during melting of a PCM contained in a horizontal cylinder. They also presented results of a numerical simulation of the melting process using a finite difference numerical method. Recently, Ng *et al.* [6] studied the free convective melting of a phase change material in a horizontal cylindrical annulus heated isothermally from the inside wall. However, no prior work exists on the problem of melting in a horizontal annulus of different cross-section.

In the present study, a Streamline Upwind/Petrov Galerkin finite element method in combination with primitive variables was employed to solve convection-dominated melting problems. Simulation was carried out for melting of a pure phase change material (*n*-octadecane) in a horizontal cylindrical annulus heated isothermally from inside. Effect of the Rayleigh number on the flow patterns within the melt and local heat transfer rate at the inner wall were examined. The main objective of this paper is to demonstrate the feasibility of a passive method to enhance melting heat transfer rates in horizontal annuli by simply inverting the container after a certain amount of melting has occurred.

Mathematical formulation

For the mathematical description of a melting or freezing process the following assumptions are made: (1) heat transfer in the PCM is conduction/convection-controlled, and the melt is Newtonian and incompressible; (2) the flow in the melt is laminar and viscous dissipation is negligible; (3) the densities of the solid and the liquid are equal; (4) the Boussinesq assumption is valid for free convection, *i.e.*, density variations are considered only insofar as they contribute to buoyancy, but are otherwise neglected; (5) the solid PCM is fixed to the adiabatic container wall during the melting process.

To account for the physics of the timewise evolution of the flow at the solid/liquid interface in fixed-grid methods, the well known enthalpy-porosity model [7, 8] is employed. Penalty formulation [9, 10] is utilised to comply with the incompressibility constraint in the momentum equation.

Based on the aforementioned assumptions, the governing equations in tensor form become:

$$u_{i,i} = 0 \tag{1}$$

$$\rho\left(\frac{\partial u_i}{\partial t} + u_j u_{i,j}\right) = \frac{1}{\gamma}(u_{i,i})_{,i} + [\mu(u_{i,j} + u_{j,i})]_{,j} - \rho g\beta(T - T_0) + Ai_i \tag{2}$$

$$\rho\left(\frac{\partial h}{\partial t} + u_j T_{,j}\right) = (kT_{,j})_{,j} + q_s \tag{3}$$

In Eq. (2):

$$A = -C(1-\lambda)^2/(\lambda^3 + b) \tag{4}$$

in which b is a small constant introduced to avoid division by zero and C is a constant accounting for the morphology of the mushy region for impure PCMs. In general b is assigned a value of 0.001. For isothermal phase change (pure PCM) C is assigned a value of $1.6 \cdot 10^6$. γ is the penalty parameter which is assigned a value of $1.0 \cdot 10^9$.

The initial and boundary conditions are:

initial conditions:

$$T(x, 0) = T^0(x) \tag{5}$$

$$u_i(x, 0) = u_i^0(x)$$

boundary conditions:

$$\begin{aligned} u_i &= \bar{u}_i(s,t) && \text{on } \Gamma_u \\ \tau_i &= \sigma_{ij} n_j(s) = \bar{\tau}_i(s,t) && \text{on } \Gamma_t \\ T &= \bar{T}(s,t) && \text{on } \Gamma_T \\ q &= -(kT_{,j}) n_j(s) = q_a(s,t) + q_c(s) + q_r(s) && \text{on } \Gamma_q \end{aligned} \tag{6}$$

Using the above numerical scheme the instantaneous temperature distributions in the PCM are obtained and the magnitude of the cumulative energy charged per unit length, Q, is calculated as a function of time. The calculation is made by computing the enthalpy of the PCM at each time increment using the solid PCM at its fusion temperature as the reference state and subtracting the enthalpy of the PCM at the beginning of the melting process. The maximum amount of energy that can be charged during the melting process is

$$Q_M = \rho A_{xy} [f_H(T_w) - f_H(T_m)] \tag{7}$$

In this work, bilinear quadrilateral elements are used to perform all computations. A source-based scheme [11, 12] is used to treat the phase change effects. A backward Euler scheme is employed to accomplish the time discretization of Eq. (2).

The aforementioned numerical model has been verified by comparison with experimental results. For detailed information on the numerical model and the test of the model please refer to Gong [13].

Results and discussion

Case 1: Type A annulus

Simulations were carried out for melting of a PCM (99% pure n-octadecane) in a cylindrical horizontal annulus with a heated inner wall. The inner wall of the tube is maintained at a constant temperature higher than the melting point of the PCM. The outer wall is adiabatic. The parameters for the computed problem are listed in Table 1. A schematic diagram of the physical model simulated is shown in Fig. 1. The Rayleigh and Prandtl numbers are based on the inside diameter of the annulus.

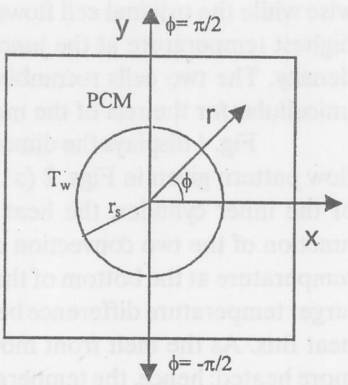

Figure 1. Schematic diagram of the physical model for type A annulus

Figs. 2 (a1, a2) and 3 (a1–a4) show the predicted contours of the isotherms (left) and streamlines (right) at various Fourier numbers for Ra = $2.844 \cdot 10^6$. At this Rayleigh number, no flow is detected in the melt region in the early stage of melting, with only one

Table 1. Parameters used in the simulation runs

Pr	Prandtl number	46.1
Ste	Stefan number	0.138
c_s/c_l	Ratio of solid/liquid specific heat	0.964
k_s/k_l	Ratio of solid/liquid heat conductivity	2.419
θ_I	Initial dimensionless temperature	–0.0256

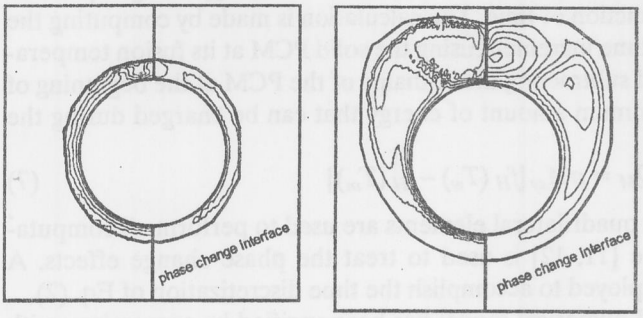

(a1) Fo = 0.0432 (a2) Fo = 0.1296

Figure 2. Isotherms (left) and streamlines (right) in the melt zone for heating from the inside

convection cell formed in the melt zone. The heat transfer rate is controlled by conduction at short elapsed times. The single convection cell splits into two cells at Fo = 0.043. The size of the second convection cell formed along the top of the heated cylinder increases with an elapsed time. The direction of the flow of the second convection cell is anti-clockwise while the original cell flows in the clockwise direction. The melt is heated up to the highest temperature at the junction of the two cells and then floats up due to its lower density. The two cells recombine at a later stage for Fo > 0.26 and thereafter remain unicellular for the rest of the melting period.

Fig. 4 displays the dimensionless heat flux distribution q/R, corresponding to the flow pattern given in Figs. 2 (a1, a2) and 3 (a2, a4). Moving from the bottom to the top of the inner cylinder, the heat flux decreases smoothly except for the troughs at the junction of the two convection cells. This is due to the fact that the melt has the lowest temperature at the bottom of the cylinder. Since the inner cylinder wall is isothermal, the larger temperature difference between the melt and the heating surface results in a higher heat flux. As the melt front moves upward along the inner cylinder, the melt becomes more heated; hence, the temperature difference between the melt and the heating surface is reduced, along with the heat flux. Now the melt at the junction between the two cells is at the highest temperature. Hence the temperature difference is lowest at the junction of the two cells, which results in a sudden drop for the heat flux. Moreover, the position of the trough is time-dependent; this is a result of the changing size of the second

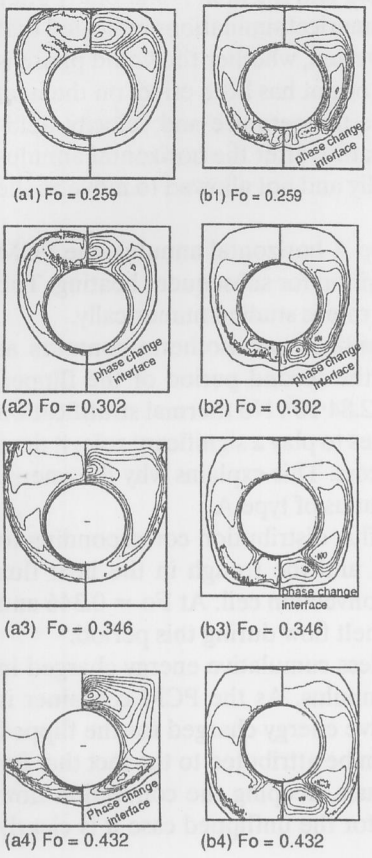

Figure 3. Isotherms (left) and streamlines (right) in the melt zone with Ra = $2.844 \cdot 10^6$ for unflipped and flipped annuli of type A

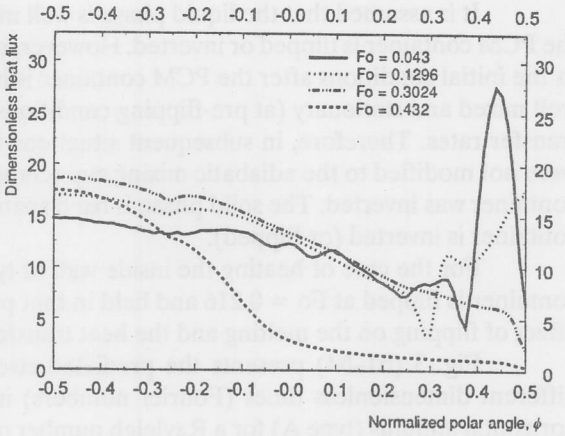

Figure 4. Local dimensionless heat flux distribution along the heated surface (Ra = $2.844 \cdot 10^6$)

convection cell with time. It can be seen from the dimensionless heat flux distribution curve (Fig. 4) that at Fo = 0.302, the two convection cells coalesce into a single cell. Thermal stratification is observed in the upper part of the melt region. The temperature gradient decreases significantly in this zone. This results in the predicted smaller heat flux in the upper half of the melt region.

Inverting the PCM container 180° about its axis is identified as a potential passive means of enhancing the heat transfer rate during the latter stages of the melting process. A schematic representing this idea is shown in Fig. 5. Numerical experiments were carried out to determine how much the heat transfer rate could be enhanced using this simple procedure.

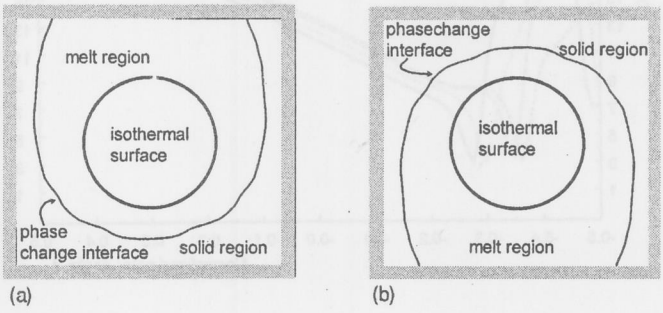

Figure 5. Schematic of the physical system for type A annulus

It is assumed that the liquid phase is well mixed and the melt is stationary after the PCM container is flipped or inverted. However, numerical simulations indicated that as the initial conditions after the PCM container is inverted, whether the liquid phase is well mixed and stationary (at pre-flipping conditions) or not has little effect on the heat transfer rates. Therefore, in subsequent situations the temperature and velocity fields were not modified to the adiabatic mixing cup temperature after the horizontal annulus container was inverted. The solid phase is fixed spatially and not allowed to move as the container is inverted (or flipped).

For the case of heating the inside wall of type A horizontal annulus, the PCM container is flipped at Fo = 0.216 and held in that position for subsequent heating. The effect of flipping on the melting and the heat transfer rate is studied numerically.

Fig. 3 (b1–b4) presents the predicted streamlines and isotherm contours at different dimensionless times (Fourier numbers) in the second period of the flipped horizontal annulus (type A) for a Rayleigh number of $2.84 \cdot 10^6$. No thermal stratification occurs in the flipped container and convection continues to play a significant role; it does not decrease during the last stage of the melting process. This explains why the energy charge rate is enhanced by flipping the horizontal annulus of type A.

Fig. 6 displays the local dimensionless heat flux distribution corresponding to the flow pattern shown in Fig. 3 (b1–b4). The crest and the trough in the heat flux distribution curve correspond to the junction of the convection cell. At Fo = 0.346 and Fo = 0.432, the single trough is a result of bicellular melt flow during this period.

Fig. 7 shows a comparison of the dimensionless cumulative energy charged in the system for both the unflipped and the flipped annulus. As the PCM container is flipped at Fo > 0.216, Fig. 7 reveals that the cumulative energy charged for the flipped case is higher than that for the unflipped case. This can be attributed to the fact that for the flipped horizontal annulus bicellular flow continues, keeping the convection flow active, thereby increasing the heat transfer rate. But for the unflipped case it is clearly

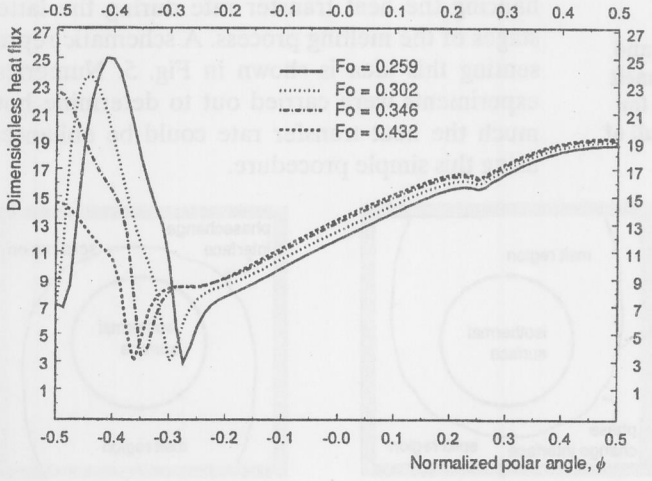

Figure 6. Local dimensionless heat flux distribution along the heated surface for flipped annuli of type A ($Ra = 2.844 \cdot 10^6$)

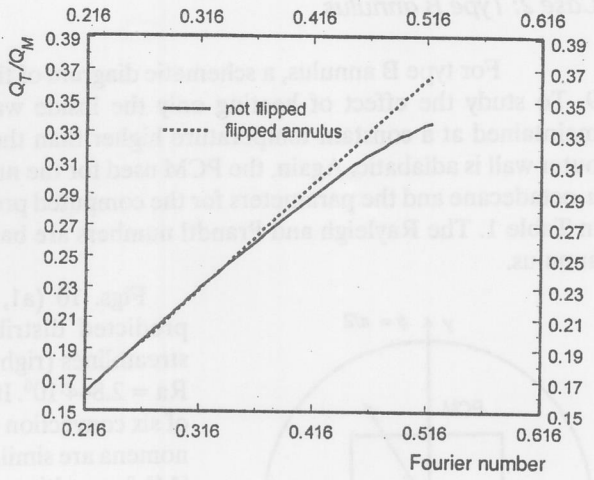

Figure 7. Comparison of dimensionless cumulative energy charge as a function of the Fourier number for type A annulus (Ra = $2.844 \cdot 10^6$)

observed in Fig. 3 (a1–a4) that thermal stratification occurs and reduces the heat transfer rate.

A comparison of the fraction melted for both flipped and unflipped horizontal annuli of type A is presented in Fig. 8. From the figure it is obvious that there is an enhancement in the melting rate with the flipped container relative to the conventional unflipped case at long elapsed times.

It should be noted that the concept of flipping at an appropriate time during the melt cycle (storage or charge cycle) may not be feasible for all design configurations of PCM storage type heat exchangers. Also, the beneficial effect of flipping appears only during the later stages of melting. Again, these results assume that the unmelted portion of the PCM is fixed (*i. e.*, not free to move during melting or upon flipping).

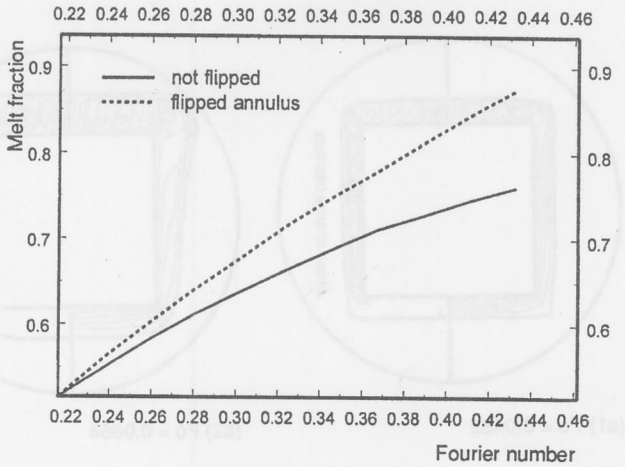

Figure 8. Melt fraction as a function of Fourier number for type A annulus (Ra = $2.844 \cdot 10^6$)

Case 2: Type B annulus

For type B annulus, a schematic diagram of the physical model is shown in Fig. 9. To study the effect of heating only the inside wall, the inner wall of the tube is maintained at a constant temperature higher than the melting point of the PCM. The outer wall is adiabatic. Again, the PCM used for the numerical experiments is 99% pure *n*-octadecane and the parameters for the computed problem are the same as those listed in Table 1. The Rayleigh and Prandtl numbers are based on the inside diameter of the annulus.

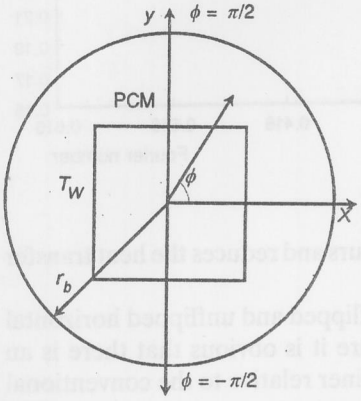

Figure 9. Schematic diagram of the physical model for type B annulus

Figs. 10 (a1, a2) and 11 (a1–a3) display the predicted distributions of isotherms (left) and streamlines (right) at various Fourier numbers for $Ra = 2.844 \cdot 10^6$. It is seen that at Fo = 0.0432 a total of six convection cells develop. The predicted phenomena are similar to those obtained by Gong *et al.* [14] for melting of a PCM in a rectangular cavity heated from below. The size of the convection cells increases and the number of cells decreases with an increase in the melt depth. The increase in the melt depth further results in the formation of a single convection cell at the top heated surface of the inner tube. At Fo = 0.26, it is found that a bicellular flow exists and that only a small portion of the PCM at the bottom remains to be melted.

Figs. 12, 13 and 14 display the dimensionless heat flux distributions $\partial\theta/\partial Y, \partial\theta/\partial X, \partial\theta/\partial Y$ along the heated bottom wall, vertical wall, and top wall respectively, corresponding to the flow patterns shown in Figs. 10 (a1, a2) and 11 (a1, a3). Moving from left to the right along the bottom heated wall the heat flux is almost constant

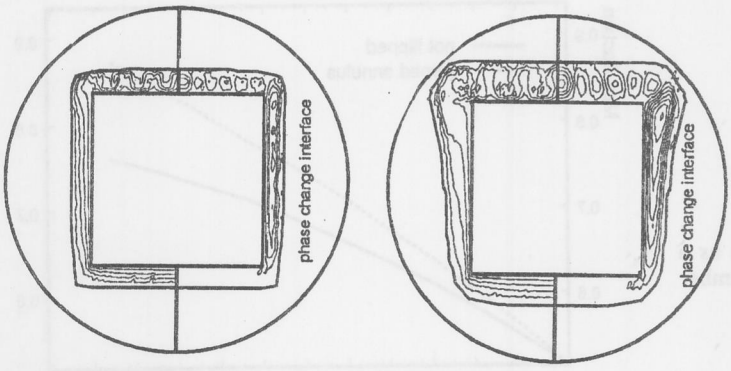

(a1) Fo = 0.0432 (a2) Fo = 0.0864

Figure 10. Isotherms (left) and streamlines (right) in the melt zone with $Ra = 2.844 \cdot 10^6$ for heating from inside

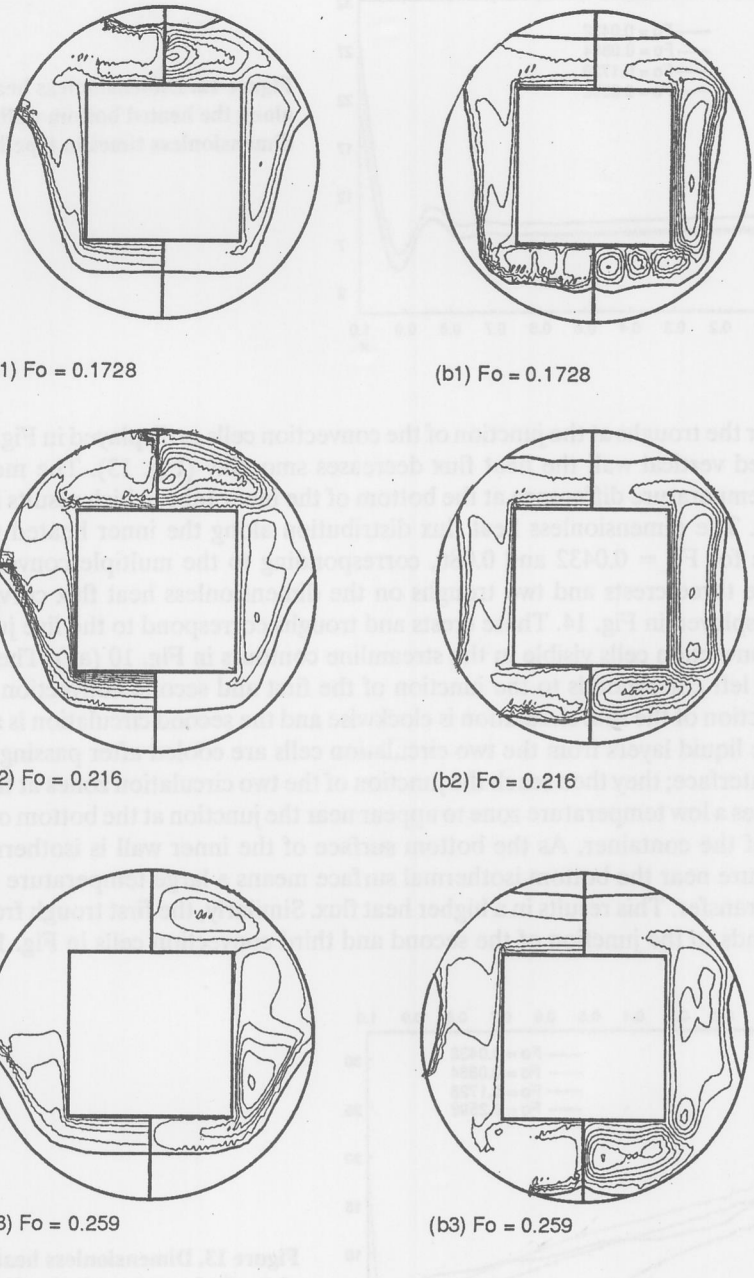

Figure 11. Isotherms (left and streamlines (right) in the melt zone with $Ra = 2.844 \cdot 10^6$ for heating from inside in case of unflipped and flipped annuli of type B

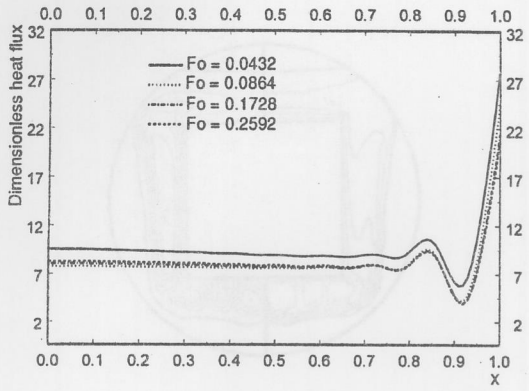

Figure 12. Dimensionless heat flux $\partial\theta/\partial Y$ along the heated bottom wall at different dimensionless times in type B annulus

except for the troughs at the junction of the convection cells as displayed in Fig. 12. Along the heated vertical wall the heat flux decreases smoothly (Fig. 13). The melt has the highest temperature difference at the bottom of the inner tube, which results in a higher heat flux. The dimensionless heat flux distribution along the inner heated top wall is wave-like for Fo = 0.0432 and 0.086, corresponding to the multiple convection cells. There are three crests and two troughs on the dimensionless heat flux curve of Fo = 0.0432 displayed in Fig. 14. These crests and troughs correspond to the five junctions of the six convection cells visible in the streamline contours in Fig. 10 (a1). The first crest from the left corresponds to the junction of the first and second convection cells. The flow direction of the first circulation is clockwise and the second circulation is anti-clockwise. The liquid layers from the two circulation cells are cooled after passing the phase change interface; they then reach the junction of the two circulation zones at the bottom. This causes a low temperature zone to appear near the junction at the bottom of the inner surface of the container. As the bottom surface of the inner wall is isothermal, a low temperature near the bottom isothermal surface means a large temperature difference for heat transfer. This results in a higher heat flux. Similarly, the first trough from the left corresponds to the junction of the second and third convection cells in Fig. 10 (a1). At

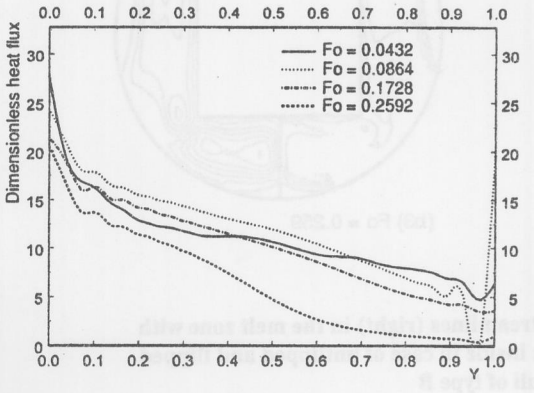

Figure 13. Dimensionless heat flux $\partial\theta/\partial X$ along the heated vertical wall at different dimensionless times in type B annulus

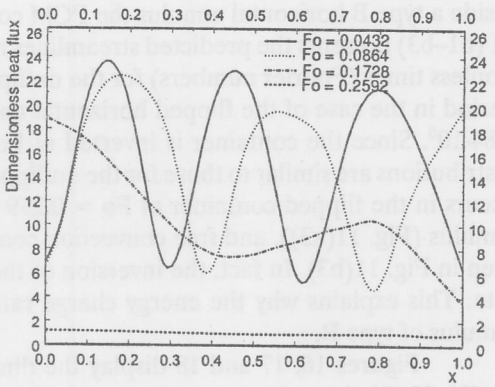

Figure 14. Dimensionless heat flux $\partial\theta/\partial Y$ along the heated top wall at different dimensionless times in type B annulus

the junction of the two cells a high temperature zone is developed which results in lower temperature difference between the wall and the melt and hence a lower heat flux.

To enhance the heat transfer rate during the latter stages of the melting process, flipping or inverting the type B PCM container at the appropriate elapsed time after melting begins is proposed as an innovative enhancement method. A schematic representing this idea is shown in Fig. 15. Numerical experiments were carried out to determine to what extent the heat transfer rate can be enhanced using this simple procedure. Moreover, it is reasonable to assume that the liquid (melt) phase is well mixed and that the melt is stationary after the PCM container is flipped or inverted and melting subsequently proceeds without any interruptions. Numerical simulations indicated that as the initial condition after the PCM container is inverted whether the liquid phase is well mixed and stationary with original temperature distribution or not has little effect on the heat transfer rate. Therefore, in subsequent simulations the temperature and velocity fields were not modified after the container was inverted.

Consider the case of heating only the inside wall of type B horizontal annulus. The PCM container was flipped at Fo = 0.13 and held in that position for subsequent heating. The effect of flipping on melting and the heat transfer rate was studied numerically.

As can be seen from the isotherms plotted in Fig. 11 (a3), thermal stratification occurs during the last stage of the melting process at Fo = 0.259. Hence for heating from

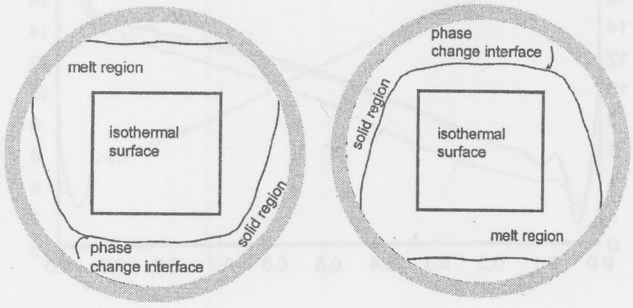

Figure 15. Schematic of the physical system for annulus type B

inside a type B horizontal annulus the PCM container was inverted at Fo = 0.1296. Fig. 11 (b1–b3) presents the predicted streamlines and isotherm contours at different dimensionless times (Fourier numbers) for the unflipped annulus (type B), and for the second period in the case of the flipped horizontal annulus (type B) for a Rayleigh number of $2.84 \cdot 10^6$. Since the container is inverted at Fo > 0.1296, the streamline and isotherm distributions are similar to those for the unflipped annulus case. No thermal stratification occurs in the flipped container at Fo = 0.259 when compared to that of the unflipped annulus (Fig. 11(a3)), and free convection continues to play a significant role as can be seen in Fig. 11(b3). In fact, the inversion of the container gives rise to a higher melting rate. This explains why the energy charge rate is enhanced by flipping the horizontal annulus of type B.

Figures 16, 17 and 18 display the dimensionless heat flux distributions $\partial\theta/\partial Y$, $\partial\theta/\partial X$, $\partial\theta/\partial Y$ along the heated bottom wall, vertical wall, and top wall for the flipped

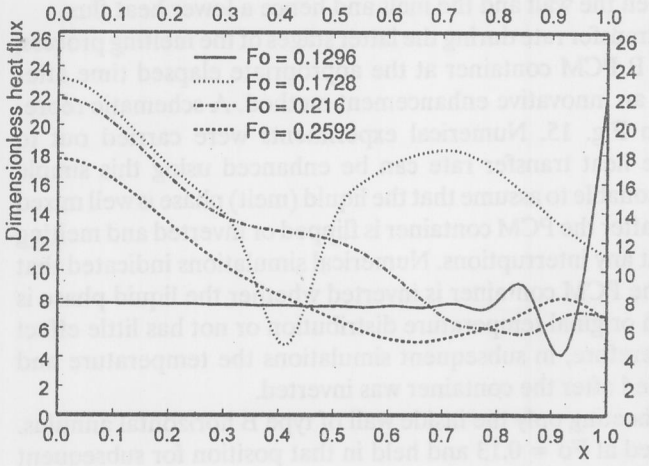

Figure 16. Dimensionless heat flux $\partial\theta/\partial Y$ along the heated bottom wall at different dimensionless times in flipped annulus of type B

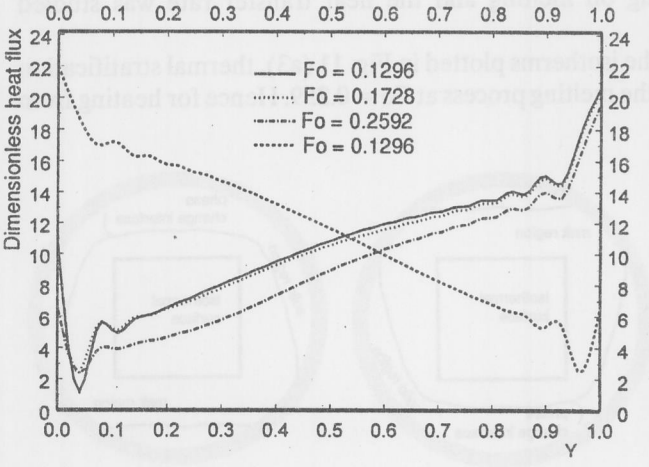

Figures 17. Dimensionless heat flux $\partial\theta/\partial X$ along the heated vertical wall at different dimensionless times in flipped annulus of type B

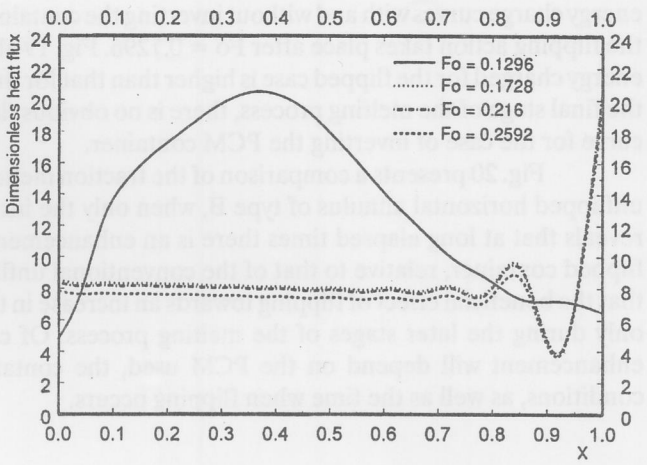

Figure 18. Dimensionless heat flux $\partial\theta/\partial Y$ along the heated top wall at different dimensionless times in flipped of type B

annulus type B respectively, corresponding to the flow patterns shown in Figures 11 (b1–b3). Along the heated bottom wall of the inner tube, the heat flux obtained for Fo= = 0.13 is the same as that obtained for unflipped annulus of type B. However, after inversion of the container the heat flux, moving from left to right of the bottom heated wall, at various Fourier numbers is found to decrease steadily. In fact, at Fo = 0.173 a trough and a crest is observed which basically corresponds to the junctions of the convection cells in Fig. 11 (b2). For the inverted container the dimensionless heat flux along the heated vertical wall increases from the bottom to the top (Fig. 17). Also the heat flux distribution along the heated top wall of the inner tube from left to right appears to be the same after inversion, as can be seen from Fig. 18.

Fig. 19 shows a comparison between the dimensionless cumulative energy charged in the system for both unflipped and flipped annuli. Prior to Fo = 0.1296, the

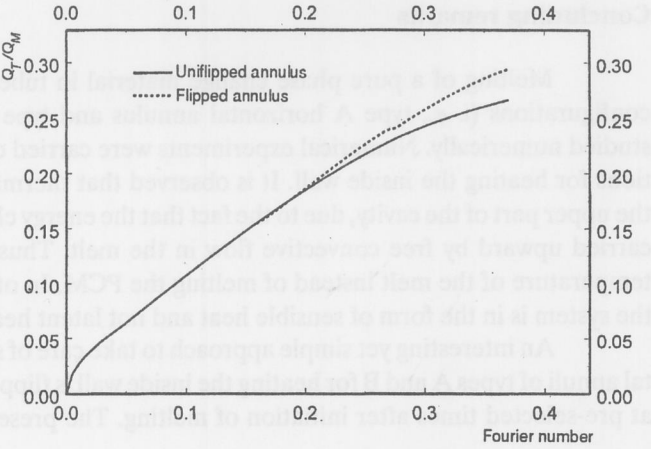

Figure 19. Comparison of dimensionless cumulative enrgy charge as a function of the Fourier number (Ra = $2.844 \cdot 10^6$)

energy charge curves with and without inverting the container are identical; this is because the flipping action takes place after Fo = 0.1296. Fig. 19 also reveals that the cumulative energy charged for the flipped case is higher than that for the unflipped case. Thus, during the final stage of the melting process, there is no obvious slow-down in the energy charge curve for the case of inverting the PCM container.

Fig. 20 presents a comparison of the fraction melted for both the flipped and the unflipped horizontal annulus of type B, when only the inside wall is heated. This figure reveals that at long elapsed times there is an enhancement in the melting rate with the flipped container, relative to that of the conventional unflipped case. It can be deduced that the beneficial effect of flipping towards an increase in the heat transfer rate is helpful only during the later stages of the melting process. Of course the magnitude of such enhancement will depend on the PCM used, the container geometry, the boundary conditions, as well as the time when flipping occurs.

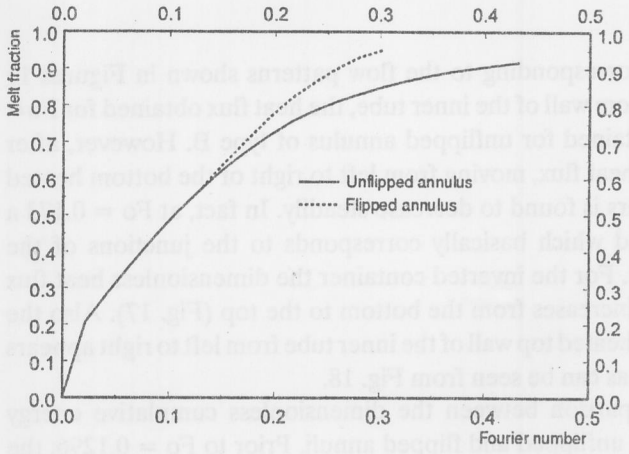

Figure 20. Melt fraction as a function of Fourier number ($Ra = 2.844 \cdot 10^6$)

Concluding remarks

Melting of a pure phase change material in tube geometries of two different configurations (*i. e.*, type A horizontal annulus and type B horizontal annulus) were studied numerically. Numerical experiments were carried out for each of the configurations for heating the inside wall. It is observed that thermal stratification is attained in the upper part of the cavity, due to the fact that the energy charged to the system is mainly carried upward by free convective flow in the melt. Thus, energy is used to raise the temperature of the melt instead of melting the PCM. In other words, energy storage in the system is in the form of sensible heat and not latent heat.

An interesting yet simple approach to take care of stratification in both horizontal annuli of types A and B for heating the inside wall is flipping or inverting the container at pre-selected times after initiation of melting. The present numerical study reveals a

good improvement in the melting rate, which indirectly reduces the melting time as compared to the conventional (unflipped) PCM container.

Acknowledgments

The authors are grateful to Natural Sciences and Engineering Research Council of Canada, Exergex Cooperation and Brossard for their support of this work via research grants.

Nomenclature

A – porosity function for the momentum equation
A_{xy} – area of a computational domain
b – a small constant
c – specific heat
C – constant
d – diameter of the inner cylinder
f_H – enthalpy-temperature function
g – gravitational force vector
h – enthalpy
k – heat conductivity
n_j – surface unit normal vector
q – heat flux
q_a – prescribed heat flux
q_c – convective heat flux
q_r – radiative heat flux
q_s – heat source
Q – instantaneous energy charged
Q_T – total energy charged
Q_M – maximum energy charged
r_s – radius of inner cylinder
r_b – radius of outer cylinder
r – radial co-ordinate (see Fig. 1)
s – boundary surface co-ordinate
t – time
T – temperature
T_0 – reference temperature
T_m – melting point of PCM
T_w – isothermal wall temperature
u_i – velocity component (second subscript means diferentiation)
X, Y – co-ordinate

Greek symbols

α – diffusivity
β – expansion coefficient
Δh – latent heat

ϕ – polar angle (see Fig. 1)
λ – porosity of a mush zone
γ – penalty parameter
Γ – boundary
μ – viscosity
ρ – density
τ_i – tangential stress components
σ_{ij} – stress tensor

Dimensionless groups

Fo – Fourier number $\mathrm{Fo} = \dfrac{t\alpha_l}{d^2}$

Pr – Prandtl number $\mathrm{Pr} = \dfrac{c_l \mu}{k_l}$

Ra – Rayleigh number $\mathrm{Ra} = \dfrac{\rho^2 c_l g \beta d^3 (T_w - T_m)}{\mu k_l}$

Ste – Stefan number $\mathrm{Ste} = \dfrac{c_l (T_w - T_m)}{\Delta h}$

θ – Dimensionless temperature $\theta = \dfrac{T - T_m}{T_w - T_m}$

Φ – Normalized polar angle $\Phi = \dfrac{\phi}{\pi}$

Superscript

$^-$ – over bar, boundary value of the variable
0 – initial value

Subscripts

l – liquid
s – solid

References

[1] Prusa, J., Yao, L. S., Melting Around a Horizontal Heated Cylinder: Part I - Perturbation and Numerical Solution for Constant Heat Flux Boundary Condition, *J. Heat. Transfer, 106* (1984), pp. 376–384

[2] Rieger, H., Projahn, U., Beer, H., Analysis of the Heat Transport Mechanisms During Melting Around a Horizontal Circular Cylinder, *Int. J. Heat Mass Transfer, 25* (1982), pp. 137–147

[3] Ho, C. J., Chen, S., Numerical Solution of Melting of Ice Around a Horizontal Cylinder, *Int. J. Heat Mass Transfer, 29* (1986), pp. 1359–1369

[4] Rieger, H., Projahn, U., Bareiss, M., Beer, H., Heat Transfer During Melting Inside a Horizontal Tube, *J. Heat Transfer, 105* (1983), pp. 226–234

[5] Ho, C. J., Viskanta, R, Heat Transfer During Inward Melting in a Horizontal Tube, *Int. J. Heat Mass Transfer, 27* (1984), pp. 705–716

[6] Ng, K. W., Devahastin, S., Mujumdar, A. S., Free Convective Melting of a Phase Change Material in a Horizontal Cylindrical Annulus, *Transactions TSTU, 4* (1998), pp. 40–52

[7] Voller, V. R., Prakash, C., A Fixed Grid Numerical Modelling Methodology for Convection-Diffusion Mushy Region Phase-Change Problems, *Int. J. Heat Mass Transfer, 30* (1987), pp. 1709–719

[8] Brent, A. D., Voller, V. R., Reid, K. J., Enthalpy-Porosity Technique for Modelling Convection-Diffusion Phase Change: Application to the Melting of a Pure Metal, *Num. Heat Transfer, 13* (1988), pp. 297–318

[9] Brooks, A. N., Hughes, T. J. R., Streamline Upwind/Petrov-Galerkin Formulations for Convection Dominated Flows with Particular Emphasis on the Incompressible Navier-Stokes Equations, *Comp. Meth. Appl. Mech. Eng., 32* (1982), pp. 199–259

[10] Dyne, B. R., Heinrich, J. C., Physically Correct Penalty-Like Formulations for Accurate Pressure Calculation in Finite Element Algorithms of the Navier-Stokes Equations, *Int. J. Num. Meth. Eng., 36* (1993), pp. 3883–3902
[11] Voller, V. R., Fast Implicit Finite-Difference Method for the Analysis of Phase Change Problems, *Num. Heat Transfer, 17* (1990), pp. 155–169
[12] Swaminathan, C. R., Voller, V. R., On the Enthalpy Method, *Int. Num. Meth. Heat Fluid Flow, 3* (1993), pp. 233–244
[13] Gong, Z. X., Time-Dependant Melting and Freezing Heat Transfer in Multiple Phase Change Materials, Ph.D. Thesis, Department of Chemical Eng., McGill University, 1997, Canada
[14] Gong, Z. X., Mujumdar, A. S., Flow and Heat Transfer in Convection-Dominated Melting in a Rectangular Cavity Heated from Below, *Int. J. Heat Mass Transfer, 41* (1998), pp. 2573–2580
[15] Hale, N. W., Viskanta, R., Solid-Liquid Phase Change Heat Transfer and Interface Motion in Materials Cooled or Heated from Above or Below, *Int. J. Heat Mass Transfer, 23* (1980), pp. 283–292
[16] Benard, H., Tourbillions cellulaires dans une nappe liquid, *Revue générale des sciences pures et appliques, 11* (1900), pp. 1309–1328
[17] Devahastin, S., Siow, S. L., Mujumdar, A. S., Effect of Inclination on Free Convective Heat Transfer During Melting of a Phase Change Material in a Rectangular Enclosure, *Applied Mechanics and Engineering, 3* (1998), pp. 491–515

Authors' address:

D. B. Khillarkar, S. Devahastin, A. S. Mujumdar
Thermal Sciences Group
Department of Chemical Engineering, McGill University
3610 University Street
Montreal, Quebec
Canada H3A 2B2

Paper submitted: February 22, 1999
Paper revised: March 10, 1999
Paper accepted: June 28, 1999